JOURNAL OF CATALYSIS 117, 202–217 (1989)

Dissociation and Oxidation of Carbon Monoxide over Rh/Al_2O_3 Catalysts

BYONG K. CHO AND CHRISTOPHER J. STOCK

Physical Chemistry Department, General Motors Research Laboratories, Warren, Michigan 48090-9055

Received February 9, 1988; revised December 22, 1988

The activity of Rh/Al_2O_3 catalysts for CO oxidation was investigated by transient isotopic pulse experiments using a packed-bed reactor. This transient experimental scheme revealed significant CO dissociation activity during CO oxidation over Rh/Al_2O_3 catalysts. Results indicate that the oxidation of CO proceeds via dissociative oxidation by its own oxygen as well as via direct oxidation by gas-phase oxygen on well-dispersed Rh/Al_2O_3 catalysts. The rate of CO dissociation is on the same order of magnitude as the rate of CO oxidation; under steady-state conditions at 300°C, the rate of CO dissociation is approximately half that of direct oxidation. Differences in CO dissociation activity between single-crystal Rh surfaces and well-dispersed supported Rh particles are explained in terms of the molecular bonding and adsorption characteristics on these two different surfaces. The importance of CO dissociation kinetics in the overall CO oxidation activity of Rh/Al_2O_3 catalysts is further discussed in view of the reaction lightoff behavior.

INTRODUCTION

The important role of Rh in the three-way control (i.e., simultaneous control of CO, NO, and hydrocarbons) of automobile exhaust emissions is rather well documented (*1*, *2*). The unique properties of Rh include its excellent activity for NO reduction as well as its superior performance for low-temperature oxidation of CO compared with Pt and Pd. However, the use of Rh in three-way catalytic converters presents a serious supply problem; that is, the Rh usage level in commercial three-way catalysts exceeds the naturally occurring mine ratio of the noble metals. In recent years a great deal of effort has been directed toward the reduction or replacement of the Rh requirement in automobile catalytic converters without sacrificing converter performance for the reduction of NO as well as for the oxidation of CO and hydrocarbons.

As to NO decomposition activity of noble metal catalysts, we have shown in a recent laboratory study (*3*) that supported Pt has catalytic activity comparable to that of supported Rh. Subsequent engine dynamometer experiments confirmed these laboratory findings; Pt/Al_2O_3 catalysts were found to have good activity for NO reduction when the air/fuel (A/F) ratio was cycled about the stoichiometric point (*4*). These observations indicate that there may exist major differences in catalytic activity in automobile exhaust between Pt/Al_2O_3 and Rh/Al_2O_3 for CO oxidation rather than for NO decomposition.

Even though the kinetics of CO oxidation on Rh has received considerable attention in recent years (e.g., (*5*, *6*)), little is known about why Rh is more active than Pt for low-temperature CO oxidation. In an effort to answer this question, we have carried out preliminary laboratory experiments in which we have discovered that during CO oxidation over well-dispersed Rh/Al_2O_3 catalysts a substantial amount of CO undergoes dissociation (or disproportionation).

Concerning the dissociation of CO on Rh surfaces, there has been some controversy in the literature for the past decade or so. Sexton and Somorjai (*7*), Castner and Somorjai (*8*), and Castner *et al.* (*9*) reported that at elevated temperatures CO dissoci-

0021-9517/89 $3.00

ated on Rh single-crystal surfaces with irregularities such as steps, kinks, and defects, whereas Thiel *et al.* (*10*) and Yates *et al.* (*11*) argued that the probability of CO dissociation on Rh(111) was negligible at 300–870 K. Marrow and Lambert (*12*) observed that the presence of surface oxygen leads to the formation of a new tightly bound form of surface CO which would presumably facilitate CO dissociation. Campbell and White (*5*), and Gorodetskii and Nieuwenhuys (*13*) observed no appreciable CO dissociation activity on polycrystalline Rh surfaces. All these studies were carried out on Rh foil or Rh single-crystal surfaces at low pressures.

For supported Rh, Yang and Garland (*14*) suggested that an irregular and well-dispersed Rh particle would favor the adsorption of two CO molecules per metal surface atom, while more regular and bulk-like Rh would favor linear and bridged CO adsorption. This agrees well with the fact that the presence of dicarbonyl species has been observed only on supported Rh surfaces and not on single-crystal Rh surfaces (*15–22*). According to Primet (*16*) Rh particles smaller than 10 Å in diameter are capable of forming $Rh(CO)_2$ species, and the appearance of the dicarbonyl complex is associated with the dissociation of CO. Results of Yao and Rothschild (*17*) indicate that 8 Å is approximately the upper limit at which $Rh(CO)_2$ species are formed, which agrees well with the observations by Primet (*16*). According to Hyde *et al.* (*23*) dicarbonyl species are formed on monoatomically dispersed Rh sites or edge sites in rafts, both of which have cationic character through interaction with the alumina support and are not active for the adsorption of oxygen.

The predominance of the dicarbonyl species on Rh/Al_2O_3 following oxidation of Rh/Al_2O_3 was also observed previously (*14, 16, 21*). Under oxidizing conditions this species gives rise to a new IR band at 2120 cm^{-1} which was assigned to a single adsorbed CO and an adsorbed O atom presumably formed as a result of CO dissociation. Recently Solymosi and Erdohelyi (*24*) observed the dissociation of CO on highly dispersed Rh at temperatures above 200°C. This has been confirmed by Zaki *et al.* (*25*) more recently. Yates *et al.* (*18*) showed that isotopic exchange between $^{13}CO(g)$ and $^{12}CO(ads)$ occurs rapidly at low temperatures (about 200 K) for $Rh(CO)_2$ species. According to the results by Vannice (*26*) supported Rh has CO dissociation activity comparable to that of supported Ni. All these observations indicate an appreciable CO dissociation rate on Rh/Al_2O_3, in accordance with our preliminary results.

The controversial literature reports on the dissociation of CO as well as the importance of CO oxidation kinetics over Rh/Al_2O_3 in automobile exhaust emission control have prompted us to examine in detail the role of CO dissociation in CO oxidation over Rh/Al_2O_3. In view of the above-mentioned literature reports on supported Rh and our preliminary findings, we felt there is a strong possibility that the dissociation of CO is an important factor in determining the overall kinetics of CO oxidation over low-loaded Rh/Al_2O_3 catalysts under atmospheric conditions. In this work we investigated the kinetics of the dissociation and oxidation of CO over Rh/Al_2O_3 using an isotopic transient experimental technique. The isotopes used in this study were ^{13}CO and $^{18}O_2$, except for a separate experiment with unsupported Rh powder using $C^{18}O$. ^{13}CO (mass number = 29) was chosen in place of CO (mass number = 28) to avoid possible interference in the mass spectrometer signal with background levels of CO and N_2 (mass number = 28 for both).

TRANSIENT PULSE EXPERIMENTS

Description of Experiments

The Rh/Al_2O_3 catalyst used in the experiments was prepared by impregnating Al_2O_3 support with $[(n\text{-}C_4H_9)_4N]_2$ $[Rh(CO)Br_4]_2$ using a nonaqueous impregnation technique (*27*) in order to obtain a shallow noble metal band near the periphery of the cata-

lyst particles. Following impregnation the catalyst was dried overnight in air at room temperature, heated slowly in flowing air up to 500°C, and then calcined in air at 500°C for 4 h. The noble metal dispersion was measured by CO chemisorption in the flow system assuming 1 : 1 stoichiometry between a surface metal atom and an adsorbed CO molecule on Rh/Al_2O_3. (We recognize that the measured noble metal dispersion may be overestimated, considering the formation of dicarbonyl species on Rh/Al_2O_3 as quoted earlier. However, the possible error involved has no effect on the interpretation of our results.)

The reactor was made of a 0.32-cm-o.d. stainless-steel tube packed with catalyst powder in a size range of 80 to 120 mesh. The detailed characteristics of the catalyst and the reactor are listed in Table 1. The reactor temperature was measured in the middle of the bed and controlled electronically with a typical precision of ±1°C. The preheating of the feed gas was achieved in a blank alumina section loaded upstream of the reactor. The gas flow rate through the reactor was measured and controlled by electronic mass flow controllers. Transient responses of the gas-phase concentration in the exit stream from the reactor were monitored as a function of time by a mass spectrometer. At a flow rate of 37 cc/min the system response time from the reactor exit to the mass spectrometer was approximately 4 s. The pressure was reduced from atmospheric pressure at the reactor exit to 0.14 kPa at the sampling port of the mass spectrometer by a capillary tube. The pressure in the vacuum chamber of the mass spectrometer was maintained at approximately 10^{-6} kPa.

Before each experimental run the reactor was pretreated with 6 vol% H_2 in He flow for 2 h at 500°C to reduce the catalyst, followed by flushing with pure He for 5 min at 500°C. (The carrier gas He (99.999%) was further purified by means of an Oxisorb cartridge.) Then, the reactor was cooled to a desired temperature in He flow and the He flow was maintained for an additional ½ h so that the reactor bed temperature reached thermal equilibrium.

TABLE 1

Catalysts and Reactor Characteristics

Support:	Al_2O_3	
	Particle size,	80–120 mesh (125–177 μm dia.)
	BET surface area,	70 m^2/g
Catalyst:	Rh/Al_2O_3	
	Rh loading,	0.09 wt%
	Rh dispersion,	91%
Reactor:		
0.32-cm (⅛ in.)-o.d. stainless-steel tubing		
	Bed depth,	1 cm
	Gas space velocity,	64,000 h^{-1} (STP)
	Temperature,	200–500°C
	Pressure,	101.3 kPa (1 atm)

The pulse duration was controlled by a universal programmable timer manufactured by Xanadu Controls. The transient response data were stored in an on-line computer and retrieved later for plotting on an X–Y recorder.

The concentrations of *CO, C*O, and $*O_2$ cylinders used in this study were 0.2, 0.2, and 0.4 vol% in He, respectively. The superscript * on the upper left corner of the atomic symbol denotes isotopes of carbon and oxygen, that is, *C for ^{13}C and *O for ^{18}O. The purity of ^{13}C atoms in ^{13}CO was 99%, while the purities of ^{18}O atoms in $C^{18}O$ and $^{18}O_2$ were 98 and 97%, respectively. A carbonyl trap made of alumina pellets was placed in the carbon monoxide flow line in order to remove possible nickel and/or iron carbonyl contamination from carbon monoxide. Standard transient experiments involved introducing to the reactor (*CO + $*O_2$) multiple pulses of 10 s in duration each with He flush for 110 s between successive (*CO + $*O_2$) pulses, as illustrated in Fig. 1. From blank test experiments it was assured that the alumina support and stainless-steel reactor wall did not contribute to the dissociation kinetics of CO under the conditions

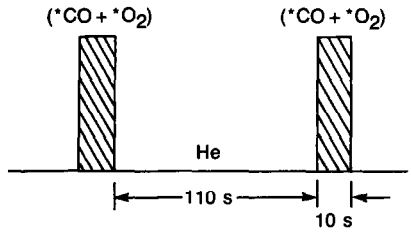

FIG. 1. Feedstream for multiple pulse experiments.

of this experiment. Later we also confirmed this by using a quartz reactor.

Transient Response during Oxidation of Catalysts

Transient activity of Rh/Al_2O_3 catalysts for the dissociation and oxidation of CO was examined by repeatedly introducing a pulse of the reactant gas mixture containing *CO and $*O_2$ into the reactor which had been pretreated with H_2. At 200°C the reactant mixture was introduced to the reactor for 10 s and then the flow was switched to pure He for 110 s before the introduction of the next pulse and so on (see Fig. 1). The reactant feedstream used here (1333 ppm for both *CO and $*O_2$) was of oxidizing stoichiometry. The degree of stoichiometric imbalance can be expressed conveniently in terms of the *stoichiometric number* (SN) defined as

$$SN = 2[O_2]/[CO], \qquad (1)$$

where SN = 1 corresponds to a stoichiometric feedstream. When SN is greater (less) than 1, the composition of the reactant pulse is net-oxidizing (net-reducing).

Taking into account the dissociation of CO there are two distinct pathways to form CO_2 from CO depending on the source of oxygen. One is *direct oxidation* of CO involving oxygen from the gas-phase O_2, and the other is *dissociative oxidation* of CO involving oxygen derived from the dissociated CO. (For the purpose of our discussions, we use the term *CO dissociation* instead of *CO disproportionation* because the latter can be treated, at least phenomenologically, as a special case of dissociation as will be discussed later.) Direct evidence for the dissociative oxidation of CO can be obtained from transient response data during the first 10 pulses shown in Figs. 2a through 2j. To our surprise the first three pulses (Figs. 2a through 2c) lead to only *CO peaks with no trace of carbon dioxide production or $*O_2$ evolution in the effluent gas

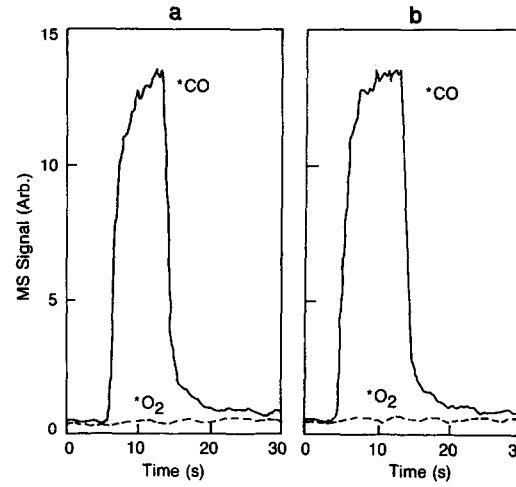

FIGS. 2a AND 2b. Transient response during oxidation of catalysts (a, pulse No. 1; b, pulse No. 2); T = 200°C; (—) *CO, (---) $*O_2$.

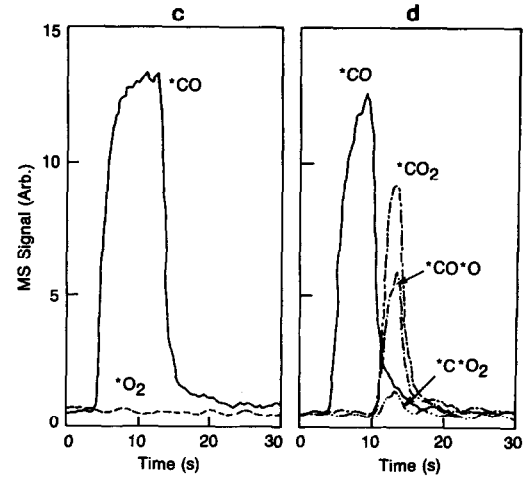

FIGS. 2c AND 2d. Transient response during oxidation of catalysts (c, pulse No. 3; d, pulse No. 4); T = 200°C; (—) *CO, (---) $*O_2$, (–––) $*CO_2$, (-•-) *CO*O, (-••-) $*C*O_2$.

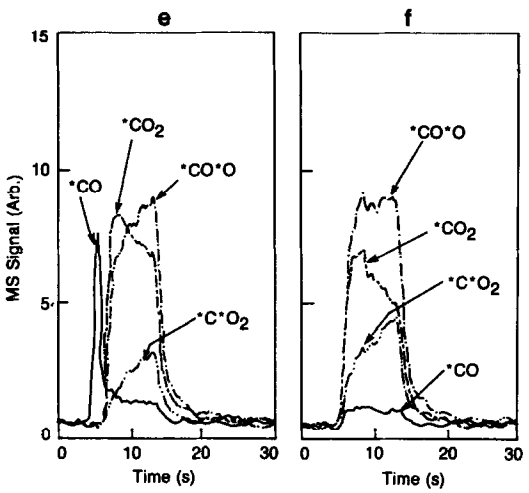

FIGS. 2e AND 2f. Transient response during oxidation of catalysts (e, pulse No. 5; f, pulse No. 6); T = 200°C; (—) *CO, (---) $*O_2$, (–––) $*CO_2$, (-●-) *CO*O, (-●●-) $*C*O_2$.

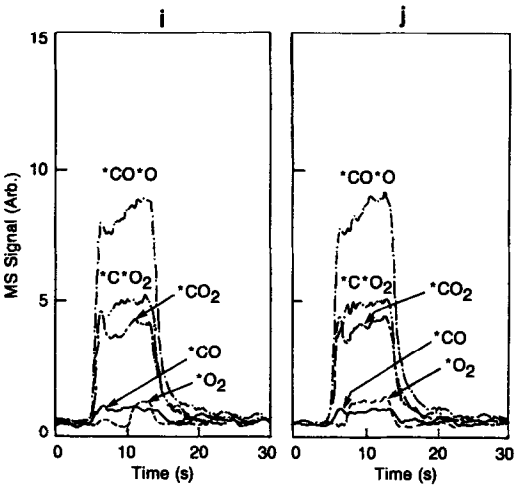

FIGS. 2i AND 2j. Transient response during oxidation of catalysts (i, pulse No. 9; j, pulse No. 10); T = 200°C; (—) *CO, (---) $*O_2$, (–––) $*CO_2$, (-●-) *CO*O, (-●●-) $*C*O_2$.

stream. (Note that $*O_2$ was introduced in excess of the stoichiometric amount in the sample pulse.) The absence of $*O_2$ in the gas phase and the lack of oxidation activity are due to the adsorption of $*O_2$ on the blank alumina particles in the preheating section and alumina support in the reactor section. This oxygen storage capability of alumina support will be further discussed later. The absence of carbon dioxide formation during the first three pulses also assures that there was no residual oxygen left on the catalyst after the H_2 pretreatment.

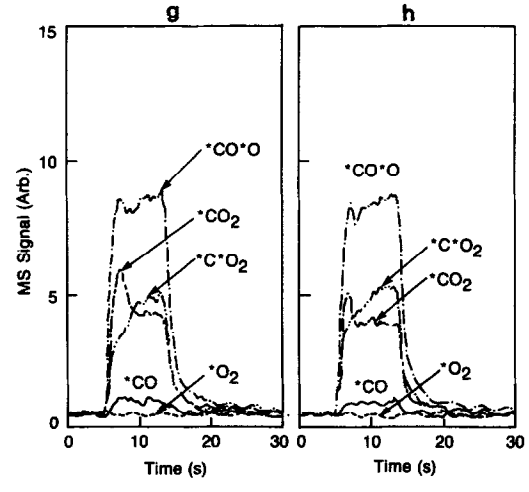

FIGS. 2g AND 2h. Transient response during oxidation of catalysts (g, pulse No. 7; h, pulse No. 8); T = 200°C; (—) *CO, (---) $*O_2$, (–––) $*CO_2$, (-●-) *CO*O, (-●●-) $*C*O_2$.

A fourth pulse (Fig. 2d) gave the first sign of *CO oxidation together with unconverted *CO. The separation of *CO from carbon dioxides is due to the chromatographic effect. Surprising in Fig. 2d is that the carbon dioxide produced is an isotopic mixture of *CO*O, $*CO_2$, and $*C*O_2$ instead of only *CO*O expected from the direct oxidation of *CO by $*O_2$.

Certainly there is a possibility that *CO*O produced from the (*CO + $*O_2$) reaction can exchange oxygen with alumina surface to yield both $*CO_2$ and $*C*O_2$ (*28–30*). However, in a separate experiment we found that the rate of oxygen exchange between carbon dioxide and alumina surface is not fast enough to explain our observations under the conditions of very high space velocity employed in this study (see Table 1). The rate of oxygen exchange between carbon monoxide and alumina surface was negligible under our experimental conditions in accordance with previous

findings (*30*). More detailed discussion on the oxygen exchange experiment will be presented later. Also, the direct exchange of oxygen between two carbon dioxide molecules according to

$$2{}^*CO{}^*O \rightleftarrows {}^*CO_2 + {}^*C{}^*O_2 \qquad (2)$$

cannot explain our observations; according to the exchange reaction, Eq. (2), the ratio of $^*CO_2$ to $^*C^*O_2$ must be always 1 : 1, in contrast to the product distribution observed in Fig. 2d. Thus, we attribute the observations shown in Fig. 2d mainly to the dissociation of *CO on Rh.

In Fig. 2d, the active reaction zone in which carbon dioxide is produced corresponds to the downstream-half of the pulse, indicating that the reactor is not yet fully activated. Upon introducing a fifth pulse (Fig. 2e) we see that reaction front moves toward the front end of the pulse indicating that a larger fraction of the reactor has been activated. The relative intensity of O*-containing products (i.e., $^*CO^*O$ and $^*C^*O_2$) increases compared with that of O-containing products (i.e., $^*CO_2$). After a sixth pulse is introduced (Fig. 2f) the reaction front sweeps through the reactor and the entire reactor becomes active for *CO oxidation. Comparison of the $^*CO_2$ peak with the $^*C^*O_2$ peak indicates that the upstream portion of the pulse is more active for $^*CO_2$ production than the downstream portion of the pulse, while this trend reverses for $^*C^*O_2$ production. Note, however, that the total amount of $^*CO_2$ and $^*C^*O_2$ stays about the same over the entire pulse. The direct oxidation rate is now almost constant over the entire pulse.

In the downstream-half of the seventh pulse (Fig. 2g), the rates of both $^*CO_2$ and $^*C^*O_2$ production remain constant, while in the upstream-half of the pulse the rate of $^*CO_2$ production is greater than that of $^*C^*O_2$ production. Overall, the region favorable for $^*CO_2$ production is getting smaller, while that for $^*C^*O_2$ production is getting bigger as the number of pulses increases as shown in Figs. 2a through 2j. After a ninth pulse (Fig. 2i) the $^*O_2$ signal starts to appear and moves downstream along the reactor as shown in Fig. 2j.

In summary, Figs. 2a through 2j clearly demonstrate that CO dissociation occurs readily on Rh/Al_2O_3 catalysts at 200°C under oxidizing conditions. This agrees very well with the previous findings by Yang and Garland (*14*), Primet (*16*), and Solymosi and Erdohelyi (*24*). In a separate experiment where the pulse contained only *CO, we observed no indication of *CO dissociation. The reasons why the presence of oxygen may enhance the CO dissociation activity of Rh/Al_2O_3 will be discussed later.

Transient Response during Reduction of Catalysts

The reproducibility of the results presented in Figs. 2a through 2j and the transient catalytic activity during a reduction period were examined by carrying out the same CO oxidation experiments as those described above up to 30 pulses and then shutting off the $^*O_2$ flow to that sample pulse. Results (maximum mass spectrometer signal for each pulse) obtained under oxidizing conditions are shown on the left side of Fig. 3, and fairly well reproduced the trends shown in Figs. 2a through 2j. When

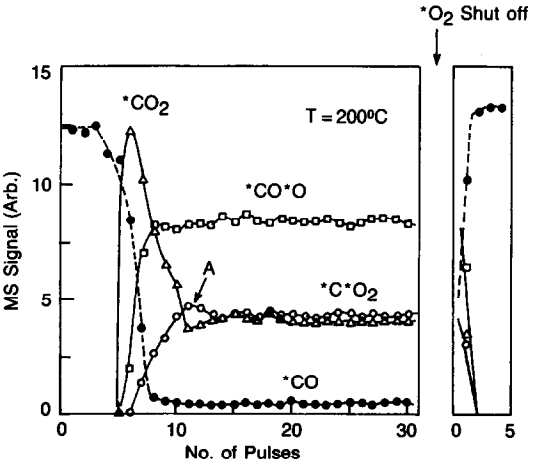

FIG. 3. Transient response during oxidation of catalysts followed by reduction of the catalysts; T = 200°C; (●) *CO, (△) $^*CO_2$, (□) $^*CO^*O$; (○) $^*C^*O_2$.

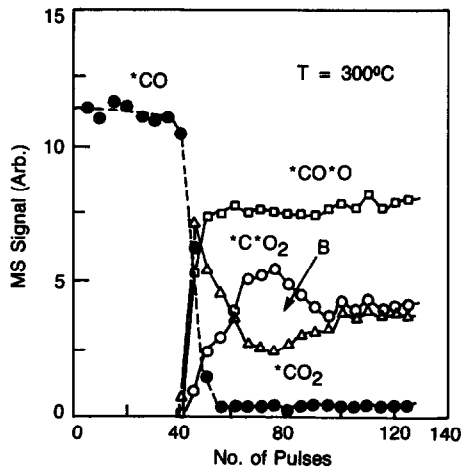

FIG. 4. Effect of catalyst temperature on the transient response; T = 300°C; (●) *CO, (△) *CO_2, (□) *CO*O, (○) *C*O_2.

the catalytic activity was well stabilized under the oxidizing condition after 30 pulses, the *O_2 flow was shut off while keeping the *CO flow constant. On the right side of Fig. 3 is presented the transient response of the catalytic activity during this reduction period. The concentration levels of *CO_2, *CO*O, and *C*O_2 all drop to zero within a couple of *CO pulses, while the *CO concentration level jumps up as can be expected. Obviously this indicates that there is no dissociative oxidation of *CO in the absence of oxygen.

It is interesting to note that the rates of *CO_2 and *C*O_2 production fluctuate before final stabilization, as shown in loop A in Fig. 3. This seemingly self-adjusting fluctuation between *CO_2 and *C*O_2 production rates becomes more apparent at higher temperatures as will be presented later.

Effects of Catalyst Temperature

Recall that all the transient response data discussed above were obtained at 200°C. The results of the same transient response experiments conducted at higher temperatures (300 and 400°C) are presented in Figs. 4 and 5. Comparing Figs. 3, 4, and 5 leads to the interesting observation that the higher the catalyst temperature becomes, the larger is the number of pulses required for the CO oxidation reaction to initiate. This observation seems reasonable in view of the two facts: first, CO oxidation does not initiate until oxygen saturates the support. Second, the alumina support has its own oxygen storage capability which increases with temperature (*3*). That is, at higher temperatures more oxygen is required to oxidize the support due to the larger oxygen storage capacity of alumina.

The overall transient behavior of the catalyst at 300°C (Fig. 4) is similar to that at 200°C (Fig. 3), except that the CO oxidation becomes rapid only after a larger number of pulses. It is important to emphasize that the reaction lightoff starts with the production of *CO_2 from the dissociative oxidation of *CO. Also noteworthy is a big rate-fluctuation loop denoted by B in Fig. 4 (cf. Fig. 3).

At 400°C (Fig. 5) the transient behavior is again similar to that at 200 and 300°C. However, instead of the sudden reaction lightoff displayed in Figs. 3 and 4, we observe more gradual carbon dioxide production in Fig. 5. It is interesting to note that after 100 pulses the production rates of *CO_2 and *C*O_2 exhibit multiple fluctuating loops (C and D in Fig. 5), whereas the production rate of *CO*O via direct oxidation has reached more or less a steady level. This

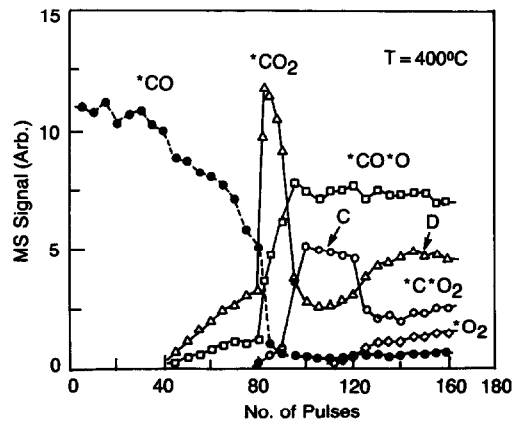

FIG. 5. Effect of catalyst temperature on the transient response; T = 400°C; (●) *CO, (△) *CO_2, (□) *CO*O, (○) *C*O_2, (◇) *O_2.

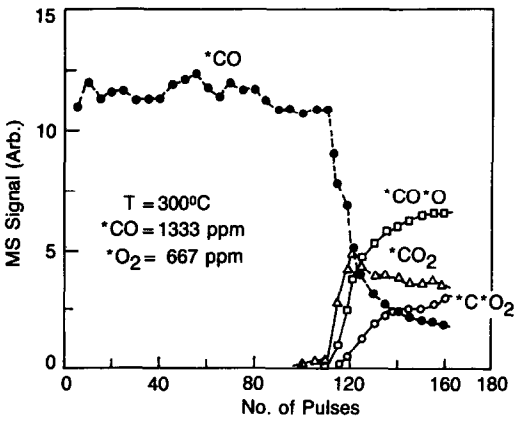

FIG. 6. Effect of chemical composition on the transient response; T = 300°C; SN = 1; (●) *CO, (△) $*CO_2$, (□) *CO*O, (○) $*C*O_2$.

rate fluctuation eventually disappeared at steady state with approximately the same production rate for $*CO_2$ and $*C*O_2$. We do not have a clear explanation for the rate fluctuation but speculate that it may be related to the accumulation of carbon on the catalyst during CO dissociation (see the discussions on the kinetic model to be proposed later). A small amount of $*O_2$ was detected as shown in Fig. 5, but *OO and O_2 signal was negligibly small.

Effect of Feedstream Stoichiometry

The effect of the stoichiometry of the reactant mixture on the transient catalytic activity was examined at 300°C. When the stoichiometric number defined in Eq. (1) is changed from 2 to 1 by reducing $*O_2$ concentration in the reactant pulse, the overall transient behavior shown in Fig. 6 is very similar to that in Fig. 4 except for the difference in scale for the number of pulses. We note that the number of pulses required for the onset of the CO oxidation in Fig. 6 is considerably larger than that in Fig. 4, which is reasonable in view of the less oxidizing reactant pulses employed in Fig. 6.

Once again we observe in Fig. 6 that the reaction lightoff is led by the formation of $*CO_2$ which is believed to be the product of dissociative oxidation.

We have observed that when a mixture of *CO and $*O_2$ is fed to the reactor, *CO oxidation does not occur until a certain number of pulses are introduced. On the other hand, CO has been shown to be the predominant surface species on Rh when a stoichiometric mixture of CO and O_2 is introduced (*6, 31*). These two observations lead us to believe that *CO adsorbs on Rh while $*O_2$ adsorbs primarily on Al_2O_3 during the transient period. When the alumina support is nearly saturated with $*O_2$, $*CO_2$ formation via dissociative oxidation of *CO occurs at the peripheral edge of the Rh particles where the dissociation of *CO is expected to proceed from dicarbonyl species (*14, 16*). As soon as the reaction lights off with the dissociative oxidation of *CO, the Rh surface starts to create vacancies which are available for the adsorption of gas-phase $*O_2$. Then follows the traditional direct oxidation of *CO on the Rh surface to produce *CO*O. This mechanistic hypothesis is in agreement with all the observations we have made so far, and suggests the importance of surface oxygen on the alumina support in initiating the CO oxidation reaction on well-dispersed Rh/Al_2O_3 catalysts.

Effect of Initial Condition of Catalysts

So far we have seen that the Rh/Al_2O_3 catalysts remain inactive for CO oxidation until they are exposed to an oxygen-containing stream. In order to see the effect of the initial condition of the catalysts, we pretreated the catalysts with 6% H_2 in He for 2 h at 500°C followed by $*O_2$ treatment for another 2 h at 500°C. Then the catalyst temperature was decreased to 300°C while the reactor was flushed with He. After a thermal equilibrium of the reactor was established at 300°C, the standard pulse experiment was resumed using (*CO + $*O_2$) pulses.

The results of such experiments (see Fig. 7a) point out three important observations. First, the CO oxidation reaction lights off immediately after the introduction of the

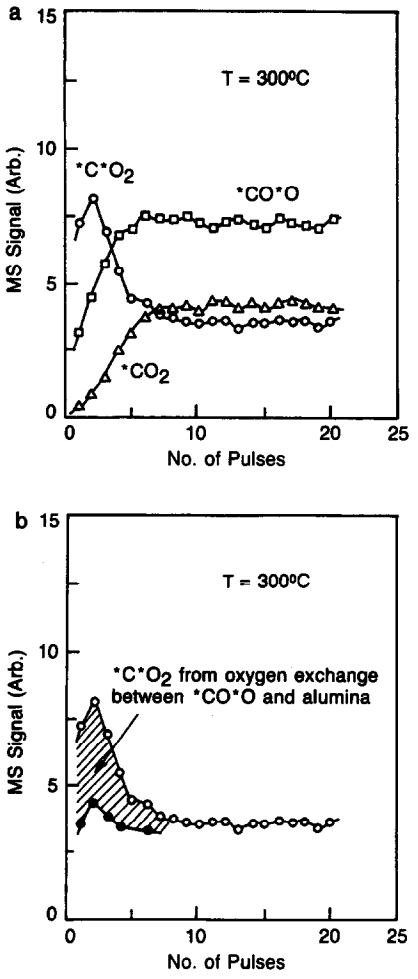

FIG. 7. (a) Effect of initial condition of catalysts on the transient response; T = 300°C; (△) $*CO_2$, (□) *CO*O, (○) $*C*O_2$. (b) Effect of oxygen exchange between carbon dioxide and alumina surface; T = 300°C; (○) $*C*O_2$ from both oxygen exchange and *CO dissociation; (●) $*C*O_2$ from *CO dissociation.

first pulse. This is quite different from the transient behavior of the reduced catalyst which exhibited a considerable induction period (see Fig. 4). Second, comparing Fig. 7a with Fig. 4 we note that the initial condition of the catalyst does not affect the steady-state behavior. The difference is observed only during the transient period. This indicates that the catalyst has a unique steady state. Third, the product distribution during the transient period is different from that of the reduced catalyst. In the case of the reduced catalyst the reaction was led by the formation of $*CO_2$ (see Fig. 4), while for the oxidized catalyst, $*C*O_2$ leads off the reaction with $*CO_2$ trailing behind. This interesting difference in product distribution during the early transient period can be explained by the oxygen exchange between carbon dioxide and alumina surface, as is discussed in the next section.

Rate of Oxygen Exchange between Carbon Dioxide and Alumina Surface

We examined the rate of oxygen exchange between carbon dioxide and alumina surface using a blank alumina column made of a 0.32-cm-o.d. stainless-steel tube. The column with the alumina bed depth of 1 cm was pretreated with 6 vol% H_2 in He for 2 h at 500°C, followed by $*O_2$ treatment for another 2 h at 500°C to saturate the alumina surface with *O. Then the column temperature was lowered to 300°C while the column was flushed with He. When the column temperature was equilibrated at 300°C, the standard pulse experiment was carried out using (CO_2 + $*O_2$) pulses instead of (*CO + $*O_2$) pulses. The exchange rate of O in CO_2 with *O on the alumina surface to form CO*O was fast initially; approximately 25% of initial CO_2 was converted to CO*O with negligible formation of $C*O_2$. However, the rate of CO*O formation decreased steadily to a negligible level within a few cycles.

This indicates that the transient overshoot in $*C*O_2$ concentration during the first few cycles of the cycling operation in Fig. 7a includes, in addition to the effect of *CO dissociation, the effect of oxygen exchange between *CO*O [produced from the (*CO + $*O_2$) reaction] and the alumina surface. When this oxygen exchange effect is appropriately accounted for in Fig. 7a, we can determine the $*C*O_2$ formation via *CO dissociation as shown in Fig. 7b. The dots in Fig. 7b represent the $*C*O_2$ formation via *CO dissociation, while the differences between the circles and the dots during the first few cycles represent the $*C*O_2$

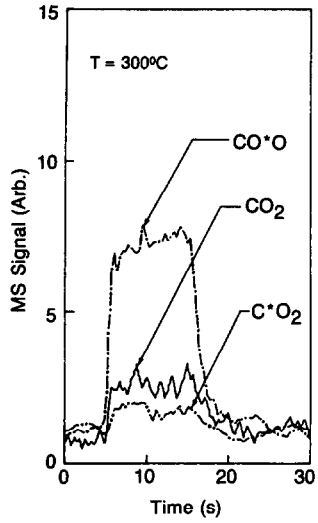

FIG. 8. Product distribution from (CO* + O_2) reaction over unsupported Rh powder; T = 300°C; (-•-) CO*O, (—) CO_2, (-••-) C*O_2.

formation via oxygen exchange between *CO*O and *O on the alumina surface. Thus, Fig. 7b indicates that the effect of oxygen exchange between carbon dioxide and alumina surface is important during the initial transient period, but becomes insignificant under the stabilized condition.

Dissociation of CO over Unsupported Rh Powder

In another separate experiment we confirmed significant CO dissociation activity during CO oxidation over Rh catalysts. To eliminate the oxygen exchange reaction due to the alumina support, we used a reactor packed with 23 mg of unsupported Rh powder in the size range 5 to 10 μm. The pretreatment and the cycling experimental procedures were the same as those used for Fig. 4, except that (C*O + O_2) pulses were used in place of (*CO + *O_2) pulses. The product distribution under the stabilized cycling condition is shown in Fig. 8, which clearly demonstrates that C*O dissociation indeed occurs on Rh without alumina support. This is in agreement with a recent study by Kellogg (*32*) and confirms the important role of CO dissociation during CO oxidation on Rh catalysts. Noting that the CO dissociation rate on Rh powder is slower than that on Rh/Al_2O_3 (compare Fig. 8 with Fig. 7a), we speculate that the CO dissociation rate may depend on the Rh particle size.

Oxygen Storage Capacity of Catalysts

The oxygen storage capacity of the catalyst was measured as a function of temperature by introducing multiple *O_2 pulses. The experiments were done for the combined reactor assembly of the blank alumina preheater and the Rh/Al_2O_3 catalysts, because of the difficulties in separating the preheater section from the reactor section after extended periods of high-temperature experiments. Because the oxygen storage capacity on Rh metal of our low-loaded catalyst is negligible compared with that on alumina support (as will be shown), this does not affect the interpretation of our data. In this experiment 1333 ppm of *O_2 was introduced to the reduced reactor assembly for 10 s followed by a relaxation period of 110 s during which He flow was maintained through the reactor assembly. While this procedure was repeated, the number of *O_2 pulses introduced to the reactor was counted until half the full *O_2 signal was detected at the outlet of the reactor.

As shown in Fig. 9 the oxygen storage effect is negligible at room temperature. However, the oxygen storage capacity increases with temperature, which is in agreement with our recent observation during NO decomposition study on Rh/Al_2O_3 (*3*) and also in agreement with the oxygen self-diffusion experiment in alumina (*33*). Above 200°C this oxygen storage effect becomes significant.

Our calculation estimates that a monolayer coverage of oxygen on Rh in this low-loaded catalyst should occur with a single pulse of oxygen. Thus, the oxygen stored on the Rh metal contributes little to the results of the oxygen storage capacity measurements presented in Fig. 9.

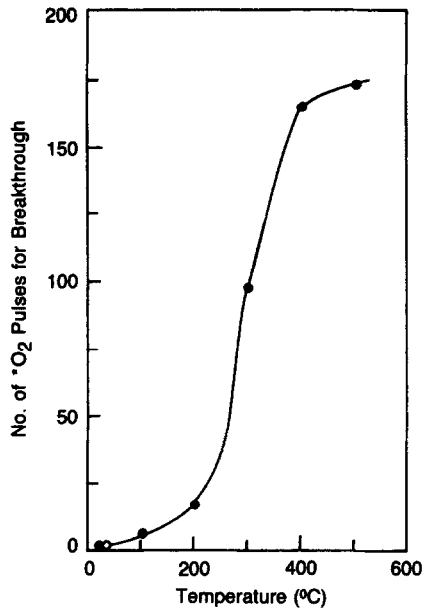

FIG. 9. Oxygen storage capacity of catalyst.

MODEL OF DISSOCIATION AND OXIDATION OF CO

Kinetic Model

Results obtained so far in this study lead us to believe that CO dissociates readily on well-dispersed Rh/Al_2O_3 above 200°C under oxidizing conditions. In this section, we propose a kinetic model which rationalizes our observations.

Traditionally, CO_2 production from CO in the absence of gas-phase oxygen has been described either by simple dissociation

$$\begin{aligned} CO &\rightarrow C + O \\ CO + O &\rightarrow CO_2 \end{aligned} \qquad (3)$$

or by disproportionation

$$2CO \rightarrow CO_2 + C. \qquad (4)$$

Note that Eq. (4) does not involve an explicit CO dissociation step. Under oxidizing conditions it is hard to distinguish the former mechanism, Eq. (3), from the latter mechanism, Eq. (4), on the basis of the kinetic data obtained in the laboratory reactor. In reality it is most likely that both mechanisms are at work simultaneously. Therefore, we propose to combine these two mechanisms into one as

$$2CO \rightarrow \alpha CO_2 + (2 - 2\alpha)\,O + (2 - \alpha)C. \qquad (5)$$

Here we introduced a parameter α, which we call a *disproportionation constant*. It is easy to see

$\alpha = 0$ for simple dissociation

$0 < \alpha < 1$ for incomplete disproportionation

$\alpha = 1$ for complete disproportionation.

The incomplete disproportionation, in which some of the dissociated oxygen does not react with another CO, may result either from the desorption of oxygen or from reduced CO mobility by the presence of other species on the surface. It should be noted here that the maximum utilization of oxygen is achieved when $\alpha = 1$. Whenever α is less than unity, the utilization of oxygen in the system to oxidize CO is less than ideal. Thus the disproportionation constant α has an important physical meaning as a measure of the efficiency of the utilization of oxygen derived from CO dissociation.

A comprehensive CO oxidation model which includes both the dissociative and the direct CO oxidation pathways is presented in Fig. 10. The rate fluctuation between $*CO_2$ and $*C*O_2$ production shown in Figs. 3, 4, and 5 can be explained on the basis of this kinetic model as follows. When

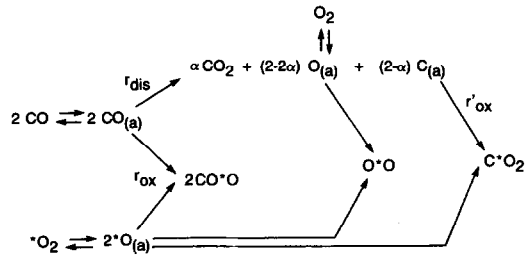

FIG. 10. Model for CO dissociation and oxidation on Rh/Al_2O_3.

*CO dissociation starts on Rh/Al_2O_3, $*CO_2$, O(a), and *C(a) form immediately. While $*CO_2$ desorbs, O(a) and *C(a) accumulate on the catalyst. As the surface coverage of *C(a) increases, $*CO_2$ production decreases due to the increased surface coverage of *C(a) while $*C*O_2$ production increases due to the oxidation of *C(a) by $*O_2$. This leads to the decrease of the surface coverage of *C(a) resulting in the decrease of $*C*O_2$ production while increasing the $*CO_2$ production. Thus, it appears that the fluctuation between $*CO_2$ and $*C*O_2$ production rates can be explained by the dynamics of *C(a) coverage on Rh/Al_2O_3 during *CO dissociation.

Estimation of Dissociation Rate

Even without knowing all the detailed kinetic parameters involved in the model presented in Fig. 10, it is possible to estimate the dissociation rate of CO from the steady-state activity measurements. Through suitable mass balance under steady-state conditions we can get

$$\frac{r_{dis}}{r_{ox}} = \frac{\alpha[CO_2] + (2 - \alpha)[C*O_2]}{2[CO*O]} \quad (6)$$

$$(2 - \alpha)[CO_2] = \alpha[C*O_2]. \quad (7)$$

Using Eq. (7) we estimate α from Fig. 4 to be close to unity. Then from Eq. (6) we estimate that

$$r_{ox} \cong 2r_{dis} \quad (8)$$

since

$$[CO*O] \cong [CO_2] + [C*O_2] \quad (9)$$

in Fig. 4. In other words, the steady-state dissociation rate of CO is approximately half the direct oxidation rate of CO at 300°C.

Note also that according to Eq. (7) the steady-state rate of $*CO_2$ production cannot exceed that of $*C*O_2$ production regardless of the rates r_{ox}, r_{dis}, r'_{ox}. This is consistent with all of our observations. The model indicates that when α is close to unity, the O_2 and O*O production is negligible. This explains why we observe $*O_2$ but not O_2 or O*O in Fig. 5.

Effect of Perturbation by NO

It is of practical interest to examine the effect of the presence of NO on the rates of CO oxidation and dissociation over Rh/Al_2O_3, for nitric oxide is another important pollutant present in engine exhaust. In this study we perturbed the reaction system by introducing 225 ppm of NO in the reactant pulse in addition to (*CO + $*O_2$). Results obtained from a step-feed experiment at 300°C are shown in Fig. 11. (During the course of this study we found out that a continuous pulse experiment becomes equivalent to a step-feed experiment, if the time-on-stream is calculated on the basis of the exposure time of the catalyst to the

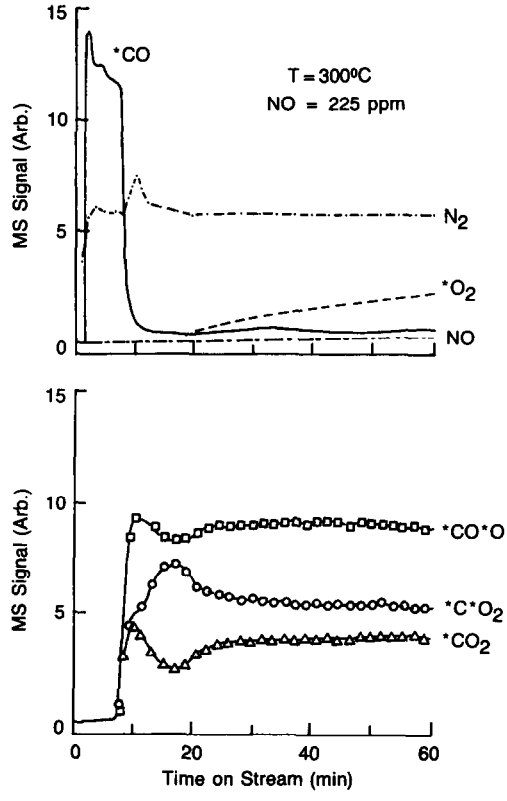

FIG. 11. Effect of perturbation by NO on the transient response; T = 300°C; [NO] = 225 ppm; (—) *CO, (-●-) N_2, (---) $*O_2$, (---) NO, (-□-) *CO*O, (-○-) $*C*O_2$, (-△-) $*CO_2$.

sample. For example, 42 pulses in Fig. 4 with 10 s in pulse duration corresponds to 7 min of the time-on-stream in Fig. 11.) Comparison of Fig. 11 with Fig. 4 indicates that the rate of $*CO_2$ formation via dissociative oxidation is severely suppressed by the presence of NO, especially during the initial transient period. At steady state the disproportionation constant α in Fig. 11 is estimated to be 0.85 using Eq. (7). This compares with 1.0 obtained from Fig. 4. The reduced value of α means that in the presence of NO the ($*CO + *O_2$) system becomes less efficient in utilizing the oxygen derived from CO dissociation.

DISCUSSION

In this work we have investigated the kinetics of CO oxidation and dissociation over Rh/Al_2O_3 catalysts using a transient experimental technique combined with isotopic tracing. This new experimental technique allowed us to obtain very interesting and potentially useful information about the detailed kinetics of CO oxidation, which could not be detected before in the traditional experimental technique under steady-state conditions. Surprisingly, the rate of CO dissociation under oxidizing conditions on well-dispersed Rh/Al_2O_3 catalysts was found to be very fast and comparable to that of the direct oxidation rate. Although the CO dissociation activity of Rh/Al_2O_3 was previously observed, its significance in the overall kinetics of CO oxidation has largely been ignored due to its supposedly small contribution compared with the direct oxidation rate. However, our data indicate that the dissociation can play an important role in determining the kinetics of CO oxidation over highly dispersed supported Rh catalysts.

Although there have been some controversies involving CO dissociation over bulk Rh surfaces for the past decade or so, there seems no such controversy in CO dissociation over well-dispersed supported Rh such as Rh/Al_2O_3. In this regard it seems appropriate to point out that on bulk Rh surfaces CO does not adsorb in the dicarbonyl form, while on well-dispersed Rh/Al_2O_3 dicarbonyl species are predominant surface species especially under oxidizing conditions. This difference in adsorption behavior between bulk metallic Rh and well-dispersed small particles of Rh appears to be a key factor in understanding their different catalytic activity toward oxidation and dissociation of CO. In the following discussions we address in more detail these differences in the behavior of supported and single-crystal catalysts.

Why Does CO Dissociate on Well-Dispersed Small Rh Particles, While It Does Not on Bulk Rh Surfaces?

There appears to be at least two reasons why well-dispersed small Rh particles can dissociate CO more easily than bulk Rh can. One reason is related to the fact that the adsorption of carbon monoxide onto a metal atom in bulk samples would result in a weaker metal–carbon bond and a stronger carbon–oxygen bond than that on isolated small particles (*34*). This can be attributed to the nature of the bonding between the surface metal atom, to which the CO is adsorbed, and its nearest neighboring atoms in the bulk sample; that is, π-bonding involving partly filled metal *d*-orbitals will occur between the metal atom in question and its nearest neighboring atoms. The carbon monoxide ligands thus will be in competition for the *d*-electrons of the central metal atom to form its own π-bond. Thus, small supported Rh particles, which do not have to engage in π-bonding with the neighboring metal atoms, permit stronger π-bonding between the metal atom and carbon monoxide. As the π-character of the metal–carbon bond increases, the bond order of the carbon–oxygen bond decreases, as evidenced by the accompanying decrease in the carbon–oxygen stretching frequency during IR spectroscopy (*34, 35*). Consequently, the adsorption of CO onto supported Rh atoms is characterized by a weaker carbon–oxy-

gen bond, facilitating the dissociation of CO.

The other reason is associated with the fact that small Rh particles in supported catalysts can adsorb dicarbonyl species while the bulk Rh surface cannot. (This may very well be related to the above π-bonding character of the bulk surface, too.) These dicarbonyl species are known to adsorb at a tilted angle of 45° from the surface normal (*18*). This tilted angle (as opposed to the surface normal position) presumably facilitates the interaction between neighboring CO molecules adsorbed on the neighboring Rh metals. This increased interaction between adsorbed CO molecules should result in faster disproportionation reaction. In fact, this kind of tilted CO on Fe and Mo surfaces has recently been identified as a precursor for CO dissociation (*36, 37*).

Why Does CO Dissociate More Easily under Oxidizing Conditions Than under Reducing Conditions on Small Rh Particles?

Among the three modes of CO adsorption—linear, bridged, dicarbonyl—on Rh/Al_2O_3, the predominance of dicarbonyl species on well-dispersed Rh particles in the presence of oxygen is now quite established. The inhibiting effects of oxygen on the linear and bridged modes of CO adsorption on Rh metal have been previously observed in the IR spectra of CO adsorbed on Rh/Al_2O_3 (*14–16, 20, 23*). Neither linear nor bridged CO existed on the surface of Rh/Al_2O_3 which was pretreated with oxygen at 500°C, and both linear and bridged CO preadsorbed on Rh/Al_2O_3 were displaced by the subsequent chemisorption of oxygen (*23*). According to Primet (*16*) pairs of CO molecules in the dicarbonyl mode ligand to Rh atoms in the 1+ oxidation state. Van't Blik *et al.* (*38*), and Solymosi and Pasztor (*39*) suggested that the Rh atoms in the 1+ oxidation state were produced by the oxidation of Rh_x by the –OH groups of the alumina support. In their EXAFS study Van't Blik *et al.* (*38*) observed that small Rh crystallites initially present in Rh/Al_2O_3 catalysts broke up into isolated Rh atoms upon CO admission, forming $Rh(CO)_2$ species. This was confirmed by Solymosi and Pasztor (*39*) in their IR study. This dicarbonyl species was more pronounced for catalysts with a low Rh loading (*14, 16, 21, 38*). On the basis of the above observations we believe that the strong CO dissociation activity of Rh/Al_2O_3 catalysts is associated with the adsorption characteristics of well-dispersed small Rh particles which tend to favor the formation of dicarbonyl species.

The strong CO dissociation activity of Rh/Al_2O_3 catalysts observed in this work may seem quite surprising to most traditional kineticists. However, our observations both on Rh/Al_2O_3 and on unsupported Rh powder are in reasonable agreement with other literature reports as discussed above. This dissociation activity appears to play an important role in the overall oxidation kinetics of CO. Thus, we believe a better understanding of the CO dissociation activity should provide guidance in the design of Rh catalysts with improved warmup performance.

Further implication of this work can be related to the fact that adsorbed sulfur has been known as a poison for CO oxidation. In this regard it should be noted that the adsorbed sulfur reduces the $d\pi$–$p\pi^*$ bonding when CO is adsorbed and thus reduces the dissociation activity of the adsorbed CO (*40*). This suggests that the poisoning effect of sulfur in CO oxidation may be partly due to the suppressed dissociation activity of CO just as the inhibition effect of NO on CO oxidation is due to the suppression of dissociative oxidation of CO as we observed in this work. These questions clearly warrant further study.

SUMMARY AND CONCLUSIONS

The activity of Rh/Al_2O_3 catalysts for CO oxidation was investigated by transient isotopic pulse experiments using a packed-bed reactor. This transient experimental

scheme revealed very interesting transient CO oxidation kinetics over Rh/Al_2O_3 catalysts. Results indicate that the oxidation of CO proceeds via dissociative oxidation by its own oxygen as well as via direct oxidation by gas-phase oxygen on well-dispersed Rh/Al_2O_3 catalysts. Differences in CO dissociation activity between single-crystal Rh surfaces and well-dispersed supported Rh particles can be explained in terms of the molecular bonding and adsorption characteristics on these two different surfaces. The importance of CO dissociation kinetics in the overall CO oxidation activity of Rh/Al_2O_3 catalysts was discussed in view of the reaction lightoff behavior. Major findings of this study are summarized below.

1. On well-dispersed Rh/Al_2O_3 catalysts a significant amount of CO dissociates under oxidizing conditions. In the absence of oxygen, on the other hand, CO dissociation activity is not significant.

2. The rate of CO dissociation is on the same order of magnitude as the rate of CO oxidation over Rh/Al_2O_3; under steady-state conditions at 300°C, the rate of CO dissociation is approximately half that of direct oxidation.

3. Results suggest that the superior CO oxidation performance of Rh/Al_2O_3 at low temperatures may be related to the high CO dissociation activity of Rh/Al_2O_3.

4. The presence of NO in the feedstream affects the product distribution of the dissociative oxidation of CO.

5. The alumina support takes up a significant amount of oxygen during CO oxidation. The total amount of oxygen that can be stored on alumina increases with temperature in the temperature range 200–500°C.

APPENDIX: NOMENCLATURE

r_{dis} dissociation rate of CO, mol/cm^2 Rh · s

r_{ox} direct oxidation rate of CO, mol/cm^2 Rh · s

r'_{ox} direct oxidation rate of C, mol/cm^2 Rh · s

SN stoichiometric number defined in Eq. (1)

Greek Letter

α disproportionation constant defined in Eq. (5)

Superscript

* isotope (*C for ^{13}C and *O for ^{18}O)

Label

(a) adsorbed state

ACKNOWLEDGMENTS

The authors gratefully acknowledge Professor W. Keith Hall and a reviewer for their suggestions during the review of this paper for the oxygen exchange experiment between carbon dioxide and alumina surface.

REFERENCES

1. Kummer, J. T., *Prog. Energy Combust. Sci.* **6,** 177 (1980).
2. Taylor, K. C., *in* "Catalysis: Science and Technology" (J. R. Anderson and M. Boudart, Eds.), Vol. 5. Springer-Verlag, Berlin, 1984.
3. Cho, B. K., and Stock, C. J., presented at the 1986 Annual Meeting of American Institute of Chemical Engineers, Miami Beach, FL, Nov. 1986.
4. Cho, B. K., *Ind. Eng. Chem. Res.* **27,** 30 (1988).
5. Campbell, C. T., and White, J. M., *J. Catal.* **54,** 289 (1978).
6. Oh, S. H., Fisher, G. B., Carpenter, J. E., and Goodman, D. W., *J. Catal.* **100,** 360 (1986).
7. Sexton, B. A., and Somorjai, G. A., *J. Catal.* **46,** 167 (1977).
8. Castner, D. G., and Somorjai, G. A., *Surf. Sci.* **83,** 60 (1979).
9. Castner, D. G., Dubois, L. H., Sexton, B. A., and Somorjai, G. A., *Surf. Sci.* **103,** L134 (1981).
10. Thiel, P. A., Williams, E. D., Yates, J. T., Jr., and Weinberg, W. H., *Surf. Sci.* **84,** 54 (1979).
11. Yates, J. T., Jr., Williams, E. D., and Weinberg, W. H., *Surf. Sci.* **91,** 562 (1980).
12. Marrow, R. A., and Lambert, R. M., *Surf. Sci.* **67,** 489 (1977).
13. Gorodetskii, V. V., and Nieuwenhuys, B. E., *Surf. Sci.* **105,** 299 (1981).
14. Yang, A., and Garland, C. W., *J. Phys. Chem.* **61,** 1504 (1957).
15. Arai, H., and Tominaga, H., *J. Catal.* **43,** 131 (1978).
16. Primet, M., *J. Chem. Soc. Faraday Trans. 1* **74,** 2570 (1978).
17. Yao, H. C., and Rothschild, W. G., *J. Chem. Phys.* **68,** 4774 (1978).

18. Yates, J. T., Jr., Duncan, T. M., Worley, S. D., and Vaughan, R. W., *J. Chem. Phys.* **70,** 1219 (1979).
19. Yates, J. T., Jr., Duncan, T. M., and Vaughan, R. W., *J. Chem. Phys.* **71,** 3908 (1979).
20. Cavanagh, R. R., and Yates, J. T., Jr., *J. Chem. Phys.* **74,** 4150 (1981).
21. Rice, C. A., Worley, S. D., Curtis, C. W., Guin, J. A., and Tarrer, A. R., *J. Chem. Phys.* **74,** 6487 (1981).
22. Dictor, R. A., presented at the 193rd National Meeting of American Chemical Society, Denver, CO, April, 1987.
23. Hyde, E. A., Rudham, R., and Rochester, C. H., *J. Chem. Soc. Faraday Trans. 1* **79,** 2405 (1983).
24. Solymosi, F., and Erdohelyi, A., *Surf. Sci.* **110,** L630 (1981).
25. Zaki, M. I., Kunzmann, G., Gates, B. W., and Knozinger, H., *J. Phys. Chem.* **91,** 1486 (1987).
26. Vannice, M. A., *J. Catal.* **37,** 449 (1975).
27. D'Aniello, M. J., U.S. Patent 4,380,510 (1983).
28. Peri, J. B., *J. Phys. Chem.* **79,** 1582 (1975).
29. Morikawa, Y., and Amenomiya, Y., *J. Catal.* **48,** 120 (1977).
30. Morikawa, Y., and Amenomiya, Y., *J. Catal.* **54,** 281 (1978).
31. Prairie, M. R., Cho, B. K., Oh, S. H., Shinouskis, E. J., and Bailey, J. E., *Ind. Eng. Chem. Res.* **27,** 1396 (1988).
32. Kellogg, G. L., *J. Vac. Sci. Technol. A* **4,** 1419 (1986).
33. Wang, H. A., and Kroger, F. A., *J. Amer. Ceram. Soc.* **63,** 613 (1980).
34. Little, L. H., "Infrared Spectra of Adsorbed Species," p. 47. Academic Press, New York, 1966.
35. Blyholder, G., *J. Phys. Chem.* **68,** 2772 (1964).
36. Moon, D. W., Cameron, S., Zaera, F., Eberhardt, W., Carr, R., Bernasek, S. L., Gland, J. L., and Dwyer, D. J., *Surf. Sci.* **180,** L123 (1987).
37. Fulmer, J. P., and Tysoe, W. T., presented at the 19th Central Regional Meeting of American Chemical Society, Columbus, OH, June, 1987.
38. Van't Blik, H. F. J., Van Zon, J. B. A. D., Huizinga, T., Vis, J. C., Koningsberger, D. C., and Prins, R., *J. Phys. Chem.* **87,** 2264 (1983).
39. Solymosi, F., and Pasztor, M., *J. Phys. Chem.* **89,** 4789 (1985).
40. Kishi, K., and Roberts, M. W., *J. Chem. Soc. Faraday Trans. 1* **71,** 1715 (1975).